RPT-O-G0035

Response of the Primary Mirror to Wind Loads

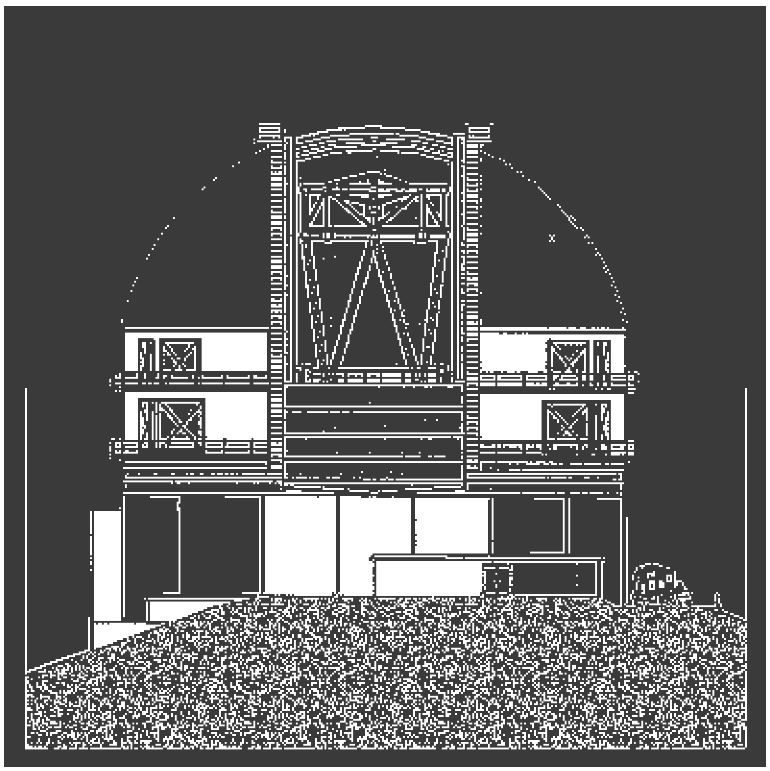

Eugene Huang

November 1993

GEMINI PROJECT OFFICE   950 N. Cherry Ave.   Tucson, Arizona 85719
Phone: (602) 325-9329   Fax: (602) 322-8590

TITLE PAGE

TABLE OF CONTENTS

RESPONSE OF PRIMARY MIRROR TO WIND LOADS

I. INTRODUCTION

The primary mirror selected for the Gemini 8-m telescope is a thin meniscus mirror 8.1m in diameter and 0.2 m thick. One of the biggest concerns is the mirror deformation under the wind load which is flushing over the primary to eliminate mirror seeing.

The wind load acting on the primary is random in nature and can be adequately characterized by an average pressure and a random fluctuating pressure. The average pressure is quasi-constant, and its effects on the image quality may be corrected with a closed loop active optics system. The random fluctuating pressure has a majority of energy in the frequency range of 0.02 to 1 hertz. The mirror deformation induced from this pressure fluctuation cannot be corrected actively because the change of mirror deformation is faster than the integration period of the active optics system (approximately 60 seconds). Therefore it is important to evaluate the mirror deformation under this wind load and to be certain that the effects on the image quality are less than the allowable error budget of 0.03 arc second at 50 % encircled energy.

This report describes the wind load, the mirror support system, the analysis methods, and the results of the predicted image degradation.

II. WIND LOAD

The wind flow approaching the mountaintop should be relatively laminar, having relatively little high frequency content. However as it reaches the surface of the mountain, and in particular as it impinges on the enclosure surfaces, turbulent flow will occur and some of the energy will be transferred to higher frequencies, even into the acoustic range. As the air flows through the telescope enclosure there will be effects not only from the direct impingement of the air flow on the mirror, but also from turbulent eddies created by local geometries of the telescope and enclosure. There will also be resonances set up by standing pressure patterns within the enclosure.

Based on a finite-difference technique, Earl Pearson (ref. 1) has developed a mathematical model to calculate the potential wind buffeting spectra at the location of the Gemini primary mirror. Many different parameters are modeled in this analysis, including the size and shape of the enclosure, the size and location of the slit opening, the area ratio of ventilation openings, the azimuth angle of wind impingement, and the orientation of the telescope. This analysis includes predicted resonances from the volume of the telescope enclosure. A typical power spectral density is shown in **Figure 1**. The integration of the area under this power spectral density curve indicates that 84 percent of the wind pressure is contributed from .02 to 1 hertz and 2 percent is

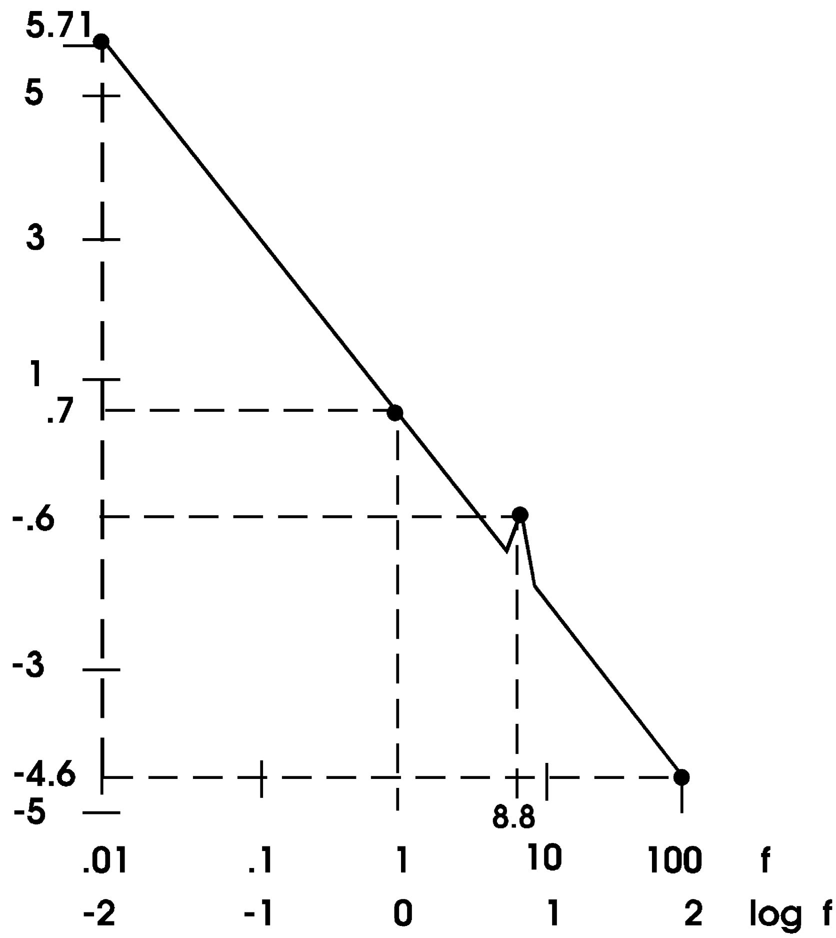

Figure 1. Pressure Spectral Density (p^2/Hz)

contributed from 1 to 10 hertz. The contribution from the frequency higher than 10 hertz is negligible.

To calculate the response of the primary mirror to this wind load, we need to know not only the wind power spectral density but also the wind pressure profile, varied spatially over the entire mirror. Experiments to obtain these data from measurements at telescope facilities on Mauna Kea are in the planning stage. In the meantime, results from other telescope projects are being used for the preliminary study. Of particular usefulness is a study done by ESO (ref. 2), in which they instrumented a plywood dummy mirror with pressure sensors. They recorded the time history of pressure variations at each of 13 locations on the mirror surface, under a number of different input wind conditions, and then derived spectra and spatial pressure variation maps from this data. The results of the normalized pressure profiles in terms of eight Zernike modes for the steady average values and the fluctuating r.m.s. values at various zenith angles (beta) and azimuth angles (alpha) are summarized as follows:

Table 1
Steady Wind Pressure Profiles

β	α	piston	def	tilt-x	tilt-y	ast-x	ast-y	tri-x	tri-y	res
0	-12	0.1395	-0.0409	0.0568	-0.0550	-0.0510	0.0488	-0.0292	0.0569	0.0519
15	-7	0.1374	-0.0940	-0.0161	0.3287	-0.1112	-0.1320	-0.0060	0.1693	0.1676
30	-6	0.2721	-0.3598	-0.0023	0.2281	0.1750	-0.0545	0.2230	-0.0582	0.2538
45	6	0.6763	-0.2625	0.1706	-0.3118	-0.1270	-0.1574	0.3264	-0.0145	0.2712
60	-15	0.8753	-0.3511	-0.1262	-0.3712	0.0628	-0.0006	0.3737	-0.1238	0.2937
75	3	1.0965	-0.4251	0.0854	-0.2413	0.1423	-0.1744	0.1829	-0.1682	0.2229

Table 2

β	α	piston	def	tilt-x	tilt-y	ast-x	ast-y	tri-x	tri-y	res
0	-12	0.1377	0.0434	0.0646	0.0545	0.0514	0.0524	0.0590	0.0431	0.0138
15	-7	0.1135	0.0878	0.0745	0.1110	0.1272	0.1015	0.1488	0.0942	0.0389
30	-6	0.0867	0.0694	0.1072	0.1335	0.1157	0.1348	0.1284	0.1486	0.0343
45	6	0.1107	0.0543	0.1407	0.0851	0.1094	0.0928	0.1055	0.0832	0.0261
60	-15	0.0873	0.0740	0.0873	0.1307	0.0922	0.1105	0.0983	0.0815	0.0255
75	3	0.1894	0.1272	0.1721	0.1389	0.1046	0.1331	0.1123	0.0826	0.0249

Fluctuating Wind Pressure Profiles

1	piston	piston
$2(x^2 + y^2) - 1$	def	defocus
x	tilt-x	tilt in x-direction
y	tilt-y	tilt in y-direction
$x^2 - y^2$	ast-x	astigmatism in x-direction
$2xy$	ast-y	astigmatism in y-direction
$x(x^2 - 3y^2)$	tri-x	triangular coma in x-direction
$y(3x^2 - y^2)$	tri-y	triangular coma in y-direction

The Zernike terms are defined as follows:

The pressure contour plots constructed from the above tables are shown in the figures B-1 thru B-12 of Appendix B.

III. MIRROR SUPPORT SYSTEM

The concept of the Gemini primary support system is shown in **Figure 2** (ref. 3). The primary mirror is supported on a uniform air pressure system, 120 axial supports and 72 lateral supports. Each axial and lateral support consists of a passive two-chamber hydraulic cylinder and an active mechanism. The active mechanism is provided to correct force errors of the hydraulic cylinder for the initial alignment and to correct the mirror figure with look up tables every 10 seconds and with closed loop feedback from a wavefront sensor every 60 seconds.

The 120 axial passive supports are divided into three groups (120 degree segment each) and hydraulically connected to each other within each group to form a statically determinate whiffletree support system. To couple the mirror to the stiff mirror cell in order to reduce the mirror deformation under wind buffeting, each group can be further divided into two subgroups (60 degree segment each) with a computer controlled valve to form an over-constrained support system. This axial support system defines the mirror in tip, tilt, and piston motions. Similarly the 72 lateral supports are divided into two groups hydraulically (180 degree segment each) and define the mirror for clocking and the decenter motion in the direction perpendicular to the trunnion axis. To define the decenter motion along the trunnion axis, six additional interconnected hydraulic cylinders are used.

This support system can be operated in three possible modes, i.e., 3-zone A, 3-zone B, and 6-zone. The two 3-zone modes have their group arrangement off-set by 60 degrees as shown in Figure 2. The reason for having three operating modes are discussed in the results section of this report. Further discussions on the defining system are given in references 4 and 5.

IV. MATHEMATICAL MODEL AND RESONANCE FREQUENCY

Using the NASTRAN finite element program, the mirror is simulated with 246 plate elements, and each support is represented by a beam and a damper element. An axial stiffness of 8800 N/mm is used for each support, and a modal damping of 5% is used for the damper. The fluid used in the hydraulic system is incompressible; therefore the sum of the displacement along the support axis for all the supports in each group must be zero. The boundary conditions for the

mir
ror
wit

Figure 2

h
the
sup

port system described above are defined by six or nine multi-point constraint (MPC) equations as follows:

Three-Zone Axial Support

$\Sigma C_i\, T_i\, (Z) = 0$ i = 1, 40 nodes at Group 1 (between θ = 30 and 150) axial supports

$\Sigma C_i\, T_i\, (Z) = 0$ i = 1, 40 nodes at Group 2 (between θ =150 and 270) axial supports

$\Sigma C_i\, T_i\, (Z) = 0$ i = 1, 40 nodes at Group 3 (between θ = 270 and 30) axial supports

$\Sigma C_i\, T_i\, (Y) + C_i\, T_i\, (X) = 0$ i = 1, 36 nodes at Group 1 (+X) lateral supports

$\Sigma C_i\, T_i\, (Y) + C_i\, T_i\, (X) = 0$ i = 1, 36 nodes at Group 2 (-X) lateral supports

$\Sigma C_i\, T_i\, (X) = 0$ i = 1, 6 nodes at X defining supports

Six-Zone Axial Support

$\Sigma C_i\, T_i\, (Z) = 0$ i = 1, 20 nodes at Subgroup 1 (between θ =30 and 90) axial supports

$\Sigma C_i\, T_i\, (Z) = 0$ i = 1, 20 nodes at Subgroup 2 (between θ = 90 and 150) axial supports

$\Sigma C_i\, T_i\, (Z) = 0$ i = 1, 20 nodes at Subgroup 3 (between θ =150 and 210) axial supports

$\Sigma C_i\, T_i\, (Z) = 0$ i = 1, 20 nodes at Subgroup 4 (between θ =210 and 270) axial supports

$\Sigma C_i\, T_i\, (Z) = 0$ i = 1, 20 nodes at Subgroup 5 (between θ = 270 and 330) axial supports

$\Sigma C_i\, T_i\, (Z) = 0$ i = 1, 20 nodes at Subgroup 6 (between θ = 330 and 30) axial supports

$\Sigma C_i\, T_i\, (Y) + C_i\, T_i\, (X) = 0$ i = 1, 36 nodes at Group 1 (+X) lateral supports

$\Sigma C_i\, T_i\, (Y) + C_i\, T_i\, (X) = 0$ i = 1, 36 nodes at Group 2 (-X) lateral supports

$\Sigma C_i\, T_i\, (X) = 0$ i = 1, 6 nodes at X defining supports

Here T_i is the translation of node i , and C_i is the proper factor for different size of hydraulic cylinder.

Modal analyses were performed for the above mirror model with a three-zone axial support and a six-zone axial support. The resonance frequencies and mode shapes are summarized as follows:

Three-Zone Axial Support

MODE	FREQUENCY	MODE SHAPE
1	11.0	decenter (rigid body)
2	15.2	astigmatism with slight tilt
3	15.2	astigmatism with slight tilt
4	18.9	clocking (rigid body)
5	25.2	decenter (rigid body)
6	25.9	defocus
7	30.9	tilt with slight astigmatism
8	30.9	tilt with slight astigmatism
9	35.1	piston with slight defocus
10	40.5	trifoil
11	40.7	trifoil
12	62.0	coma
13	62.0	coma
14	70.2	second order astigmatism
15	70.2	second order astigmatism
16	103.8	second order coma

Plots of mode shapes and surface contours for the elastic modes are shown in figures C-1 thru C-16 of Appendix C.

Six-Zone Axial Support

MODE	FREQUENCY	MODE SHAPE
1	11.0	decenter (rigid body)
2	18.9	clocking (rigid body)
3	25.2	decenter (rigid body)
4	25.9	defocus
5	30.7	astigmatism
6	30.7	astigmatism
7	30.9	tilt with slight coma
8	30.9	tilt with slight coma
9	35.1	piston with slight defocus
10	40.7	trifoil
11	48.5	trifoil
12	62.3	coma
13	62.3	coma
14	70.9	second order astigmatism
15	70.9	second order astigmatism
16	104.3	second order coma

Plots of mode shapes and surface conters for the elastic modes are shown in figures C-17 thru C-32 of Appendix C.

It is seen that the mirror with 3-zone support has the first elastic mode of astigmatism at 15.2 hertz. The mirror with 6-zone support has the first elastic mode of defocus at 25.9 hertz as the astigmatism mode increases its frequency to 30.7 hertz. The rest of the modes have nearly the same frequencies in either type of supports, except that one of the trifoil modes increases from 40.5 hertz in a 3-zone support to 48.5 hertz in a 6-zone support.

V. RESULTS OF MIRROR DEFORMATION

Mirror Deformation Under Steady Wind Pressure

The steady wind pressure is quasi static. The mirror deformation under this part of the wind load can be determined from a static analysis. This steady deformation can be corrected by the closed loop active optics. Therefore there is a minimum effect to the image degradation. However the amount of active force required to make the correction needs to be calculated for the design of the active mechanism.

For a mirror supported on a distributed passive hydraulic support system, the mirror response to an uneven wind pressure depends not only on the wind pressure profile but also on the relative orientation between the pressure profile and the distributed axial support pattern. A more uneven wind pressure, having the maximum pressure near the edge of the profile, yields a worse mirror deformation. For a same pressure profile the mirror has the worst deformation when the pressure profile is distributed on the mirror such that the maximum pressure is located between two axial support groups; and the mirror has the least deformation when the maximum pressure is at the middle of an axial support group. These will be referred to as the worst case and the best case orientations respectively in the rest of this report.

Table 3 summarizes the results of mirror deformations for the worst steady wind pressure profile given in Table 1 (beta = 15, alpha = -7 , Figure B-2). In the calculation a scale factor is used so that the r.m.s. pressure over the mirror is equal to 8 pascal.

Table 3

Support Type		R.M.S. Surface Error (nm) after correction of				Maximum Active Force Required (N)
		none	tip-tilt	focus	high order	
3-zone						
	best case	797	489	479	0.9	15
	worst case	810	728	722	1.3	24
6-zone						
	best case	369	161	128	0.3	5
	worst case	372	165	134	0.3	5

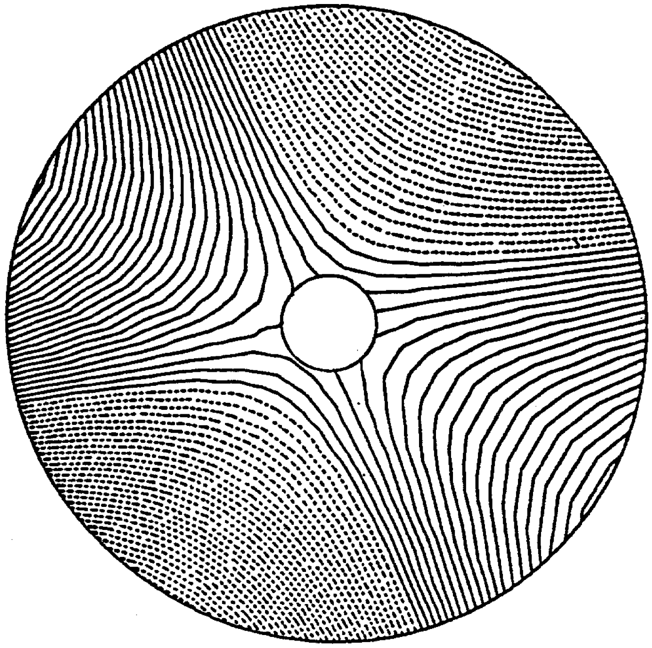

Figure 3

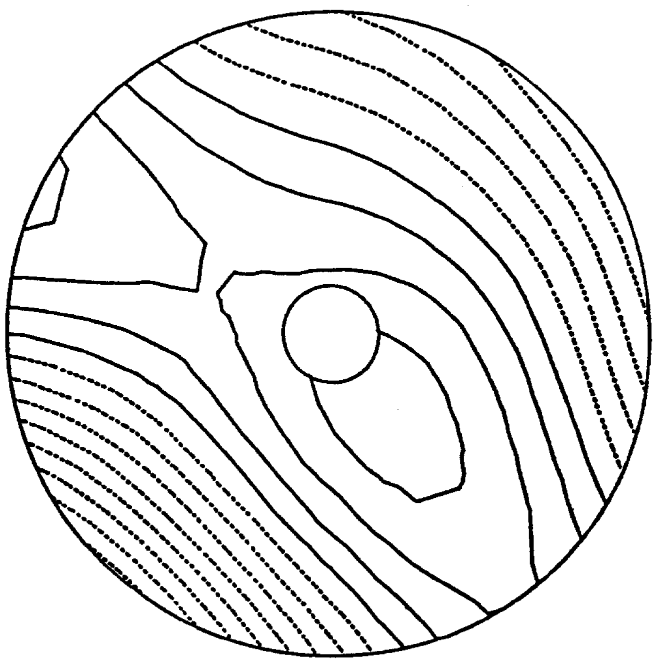

Figure 4

It is seen that the mirror deformation before correction is about two times less for the 6-zone support than for the 3-zone support. This surface error is first corrected by the motion of the secondary for the tip-tilt and defocus, and then corrected by the primary active optics for the high order errors. **Figures 3 and 4** show the contour plots of the mirror deformation after tip-tilt correction, under the worst case wind load, for the 3-zone support and the 6-zone support respectively. The deformation in the 3-zone support is dominated by the astigmatism; while the deformation in the 6-zone support shows some defocus error as well as astigmatism. The reason is that the first elastic mode for the 3-zone support is an astigmatism mode (Figure C-2) and the first elastic mode for the 6-zone support is a defocus mode (Figure C-20). The worst r.m.s. surface error after higher order correction by the primary active optics is 1.3 nm, which requires a maximum active force of 24 newtons. These error and force requirements are well within the allowable budgets. Note that this calculation does not include the wavefront sensor error which has separated error budgets.

Mirror Deformation Under Fluctuating Wind Pressure

Using the NASTRAN finite element program, a random vibration analysis was carried out for the worst case fluctuating wind load from Table 2. The results of r.m.s displacement responses at the mirror were compared to those obtained from a static analysis using the same pressure pattern. The comparisons conclude that the mirror deformation can be predicted from a static analysis because the wind load has a negligible energy content at the resonance frequencies of the mirror. This is described in Appendix A.

To calculate the response of the primary mirror to fluctuating wind pressure, both the temporal variation and the spatial variation are needed. The information in Table 2 describes the spatial distribution of the temporal r.m.s. of the pressure variations measured by ESO. At the time of this study, we do not have information about the temporal correlation between the pressures at different sensors. The Zernike coefficients in Table 2 express the pressure patterns that would have existed if the variations were correlated perfectly, that is, if the pressures peaked at all sensors at the same time. In general this assumption yields a conservative result, and these pressure patterns provide useful conditions for comparison of the performance of the 3-zone and 6-zone support system.

.

Analyses were carried out statically for all the loading conditions given in Table 2. In the calculation a scale factor is used so that the r.m.s pressure over the mirror is 2.5 pascal r.m.s. for each load case. The results of mirror deformations are summarized in Table 4. It is seen that the wind pressure profile at beta = 30 and alpha = -6 produces the worst mirror deformation. The least mirror deformation occurs at beta = 0 and alpha = -12. This deformation cannot be corrected by the primary active optics because the change of deformations is faster than the integration period of the active optics system. However, part of this surface error can be compensated by the motion of the secondary mirror at 40 hertz for the tip-tilt error and at 1 hertz for the defocus error. The surface error after tip-tilt correction and after the defocus correction are also included in Table 4. Note that there is a 30 to 50 % defocus correction for a 6-zone support, while the correction for a 3-zone support with worst case orientation is small. Also the mirror deformation is about three to nine times less for the best case orientation than for the worst case in a 3-zone support, while there is almost no difference for a 6-zone support. The worst error after corrections for a 6-zone support is about five times less than that for a 3-zone support. **Figures 5 and 6** show the contours of the wavefront error after the defocus correction for the 3-zone and 6-zone support respectively. Both of them show an error dominated by astigmatism.

Table 4

Load case beta	alpha	Support Type		R.M.S. Surface Error (nm) after correction of none	tip-tilt	focus	Image Deg. at 50% E.E. (arc-sec)	Error Budget (arc-sec)
0	-12	3-zone	best case	69	42	22	0.010	
			worst case	176	159	155	0.068	0.030
		6-zone	best case	66	47	30	0.013	
			worst case	66	47	30	0.013	
15	-7	3-zone	best case	153	128	111	0.049	
			worst case	325	294	287	0.127	0.031
		6-zone	best case	115	89	64	0.028	
			worst case	115	89	64	0.028	
30	-6	3-zone	best case	142	113	89	0.039	
			worst case	407	366	360	0.158	0.034
		6-zone	best case	138	102	74	0.033	
			worst case	139	103	75	0.033	
45	6	3-zone	best case	126	61	29	0.013	
			worst case	321	289	284	0.125	0.041
		6-zone	best case	116	75	51	0.022	
			worst cae	117	75	52	0.023	
60	-15	3-zone	best case	129	94	68	0.030	
			worst case	347	313	306	0.135	0.053
		6-zone	best case	123	90	62	0.027	
			worst case	124	90	62	0.027	
75	3	3-zone	best case	114	74	43	0.019	
			worst case	262	236	229	0.101	0.084
		6-zone	best case	102	74	44	0.019	
			worst case	102	74	44	0.019	

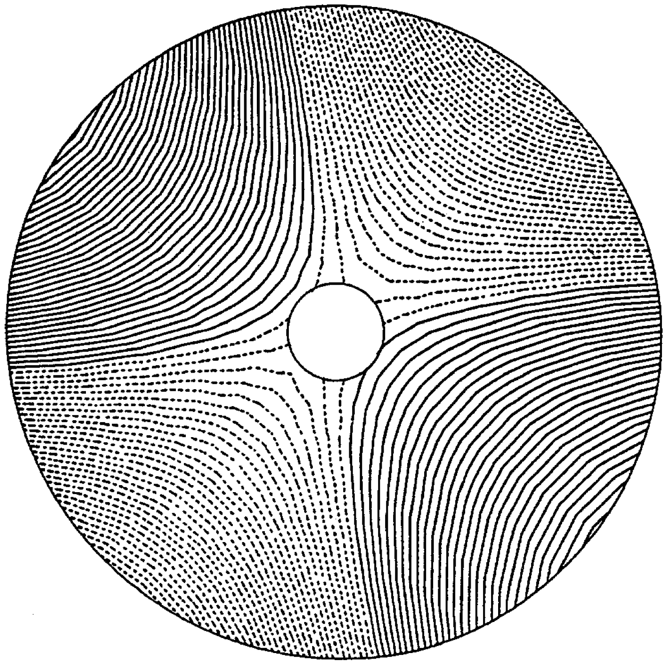

Figure 5

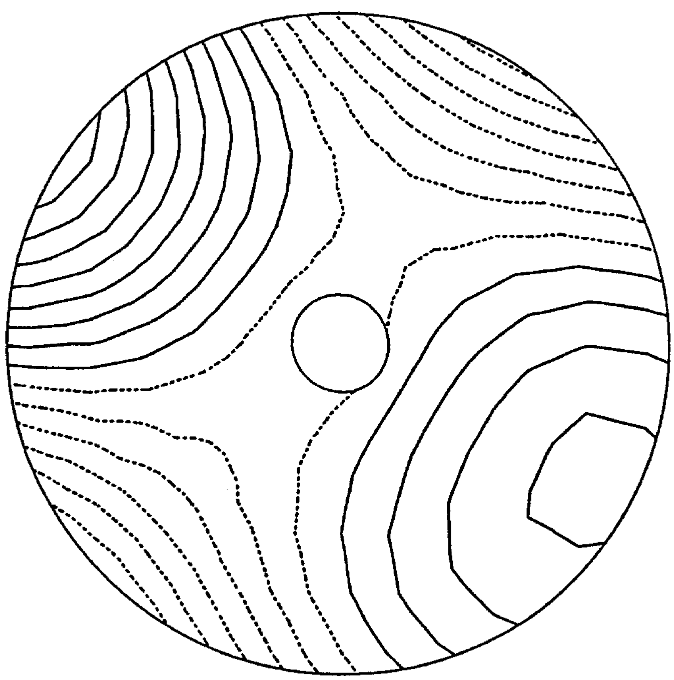

Figure 6

At zenith, the error budget for wind buffeting is 0.03 arc-second at 50 % encircled energy. This allows a surface error of about 68 nm r.m.s. when the wavefront error is dominated by astigmatism. The allowable is higher as the zenith angle increases. The results summarized in Table 4 indicate that the primary mirror with a 6-zone support is able to meet the image requirement in all the conditions for a 2.5 pascal r.m.s. fluctuating wind pressure, and under most conditions a much higher pressure fluctuation could be allowed.

In view of the three to nine times deformation difference between the best case and the worst case for a 3-zone support, the option for clocking the 3-zone support by 60 degrees, depending on the wind condition, is likely to meet the image requirement in most of the conditions. Therefore, it is highly desirable to incorporate this option in the support design by simply adding a valve between each support group as shown in Figure 2.

Support Stiffness Effects

The above analysis is based on an axial support design whose stiffness of each axial support is 8800 N/mm. A study of the mirror deformation with various support stiffness was made for the worst case wind load (beta = 30 and alpha = -6). The results are shown in **Figure 7**. As we expected, the mirror deformation is independent of the support stiffness for a 3-zone whiffletree support system. For a 6-zone over-constrained support system the mirror deformation decreases as the support stiffness increases. The effects to the performance are small for the support having a stiffness between 5000 to 12000 N/mm.

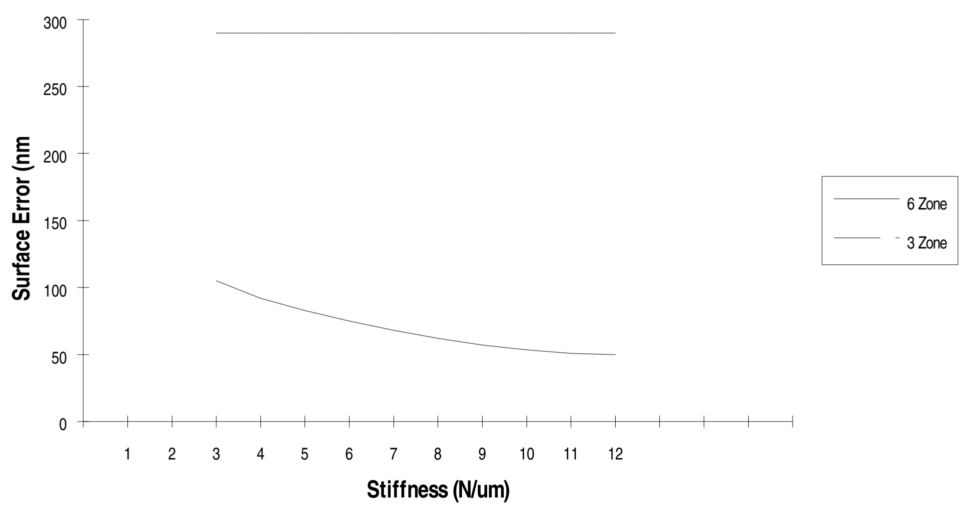

VI. CONCLUSIONS

Based on the above analysis we arrive at the following conclusions:

- A steady wind pressure of 8 pascal r.m.s acting on the primary requires a maximum 24 newton active optics force to correct the mirror deformation. The allowable steady wind pressure allowable is limited by the active optics force budget instead of the image quality error budget. With active optics correction, the steady wind pressure is not a problem up to the operating wind speed limit of 20 m/sec.

- For a 2.5 pascal r.m.s. fluctuating wind pressure acting on the primary, the worst case surface error after the secondary correction is 75 nm r.m.s. for a 6-zone support, and is 360 nm r.m.s. for a 3-zone support. The 6-zone support system improves the performance by a factor of 5 from a 3-zone support.

- In a 3-zone support system the mirror deforms three to nine times less in the best case orientation than in the worst case. Therefore an option for clocking the 3-zone support system by 60 degrees should be included in the support system design.

- For a 6-zone over-constrained support system, the mirror deformation under the wind load depends on the stiffness of the axial support. The effect on the performance is small for the support having a stiffness between 5000 to 12000 N/mm.

VII. CORRELATION OF PERFORMANCE WITH WIND SPEED

The 6-zone support system clearly performs better than the 3-zone system. This is to be expected, because in general the amplitude for a given bending mode is inversely proportional to the square of the frequency of that mode. Since astigmatism dominates the mirror bending under wind loading, and the 6-zone system has doubled the frequency for the astigmatic bending mode, the bending would be expected to reduce by a factor of four. In addition, it has been assumed that the proposed 1 Hz focus system can remove most of the defocus aberration that would be produced. These two factors together indicate a factor of 5 reduction would be expected, and the calculated results bear this out. The increased allowance on wind speed with the six zone support is therefore a factor of the square root of five.

Reference 2 states, " for the effects of wind induced deformations of the primary mirror the maximum tolerable wind speed for the VLT mirror for an open air operation is of the order of 2.5 m/sec." The ESO mirror is slightly thinner than the Gemini mirror, but Zerodur is stiffer than ULE, and the two mirrors have the same bending stiffness within 4%. The ESO specification limits mirror surface deformation to 75 nm r.m.s., which is equal to the Gemini error budget allowance at a zenith angle of 30 degrees, which appears to be the worst case zenith angle, converted into nanometers. Therefore, based on ESO's measured data, the allowable wind speed for open air operation of the Gemini mirror is 2.2 x 2.5 = 5.5 meter per second.

Based on water tunnel testing, it is expected that the wind speed at the location of the primary mirror can be controlled between 25% and 80% of the external wind speed, by adjusting the ventilation louvers on the enclosure. Therefore, it should be possible to keep the wind speed at the mirror below 5.5 m/sec for external wind speeds up to the operating limit of 20 m/sec.

One cautionary note. This calculation assumes wind turbulence comparable to an open air operation. If the enclosure introduces unusual air turbulence, for example, because of sharp edges on ventilation openings, the allowable wind speed past the primary mirror would be somewhat lower.

VIII. REFERENCES

1. " Wind Buffeting Spectra at Gemini Primary Mirror ", (*in progress*) E. Pearson, Gemini Project.

2. " Pressure Measurements with a Dummy Mirror and the Implications for the Design of the Enclosure and the Support of the Primary Mirror of the VLT ", L. Noethe etc. , European Southern Observatory.

3. "Conceptual Design of the Primary Mirror Cell Assembly", (RPT-O-G0025) L. Stepp et al., Gemini Project.

4. "The Distributed Defining System for the Primary Mirror", (RPT-O-G0029) L. Stepp et al., Gemini Project.

5. "Primary Mirror Forces from a Distributed Hydraulic Axial Support System", (RPT-S-G0038) E. Pearson, Gemini Project.

APPENDIX A

Random Vibration Analysis

1.0 Introduction

The response of the primary mirror to a random fluctuating wind pressure is a random vibration problem. A mirror with 3-zone axial supports under the worst case fluctuating wind condition (beta = 30, alpha = -6) will be examined here to understand the dynamic effects.

2.0 Analysis Method

Using the NASTRAN finite element program, the response of the mirror to the random fluctuating wind pressure is determined by applying the r.m.s. pressure profile (figure B-9) on the mirror model , described in section 4.0, with the pressure power spectral density as shown in Figure 1. To have the worst loading condition, the maximum r.m.s. pressure is located between two support groups. Model damping of 0.5% for the mirror and 5% for the hydraulic support are used.

In NASTRAN, a random vibration analysis is performed using a four part process. First, a normal modes analysis is performed to calculate the natural frequencies and mode shapes for the system within a selected frequency band of interest. In this case, all vibration modes up to a frequency of 64 hertz were calculated.

The second step is to perform a modal frequency response solution using the modes calculated in the first step. Transfer functions are calculated between each loading point and each selected output quantity (displacement, acceleration, stress, etc.). The loading points are the degrees of freedom in the model where a wind pressure is applied. NASTRAN calculates the equivalent nodal forces from the distributed pressure.

The third step is to calculate the response power spectral density for each output request. Assuming that the random loading at each node is statistically independent from the loading at any other node, the response power spectral density at each selected output is equal to the sum of the transfer function squared multiplying the input power spectral density of all the loading points.

The last step is to calculate the response r.m.s. quantity at each output request. The response r.m.s. value is equal to the square root of the integration of the response power spectral density over the entire frequency band.

3.0 Results

Figures A-1 thru A-6 show the displacement response power spectral density functions at grid points 3212, 3090, 3005, 3010, 3107, and 3223 across the mirror surface. It is seen that the shape of the curves are all identical to the input power spectral density for the frequency up to 10 hertz. This is because the first elastic resonance frequency of the mirror is 15 hertz and there is no dynamic amplification below 10 hertz.

The r.m.s. displacement responses are obtained from integrating these curves over the frequency range of 0.01 to 10 hz and 0.01 to 64 hz. The results are summarized in Table A-1. This indicates that the r.m.s displacement response contributed from the input higher than 10 hertz is less than 1 %.

The displacements calculated from a static analysis by applying the r.m.s. wind pressure on the mirror statically are also included in Table A-1 for comparison. It is seen that the deviations are less than 4 %. Further comparisons for the rest of grid points on the mirror show similar results.

The above comparisons indicates that the mirror deformation can be predicted from a static analysis because the wind load has a negligible energy content at the resonance frequency of the mirror.

Table A-1

Location grid (r, θ)	R.M.S. Displacement Response (nm)		
	.01 to 10 hz	.01 to 64 hz	Static
3212 (4050,155)	1125.6	1126.4	1115.6
3090 (2362,157)	543.3	543.7	540.0
3005 (600,165)	81.6	81.9	80.6
3010 (600,315)	26.5	27.2	26.2
3107 (2362,322)	48.4	48.5	48.1
3223 (4050,325)	221.9	222.3	220.7

APPENDIX B

Contour Plots Of Wind Pressure Profiles

APPENDIX C

Plots of Mode Shapes and Surface Contours